applied sciences

MDPI

Article

Optimized Planning of Power Source Capacity in Microgrid, Considering Combinations of Energy Storage Devices

Zifa Liu [1], Yixiao Chen [1,*], Ya Luo [1], Guankun Zhao [1] and Xianlin Jin [2]

[1] School of Electrical and Electronic Engineering, North China Electric Power University, Beijing 102206, China; zifaliu@ncepu.edu.cn (Z.L.); luoyaturbo@ncepu.edu.cn (Y.L.); 1141181127@ncepu.edu.cn (G.Z.)

[2] Guohua Energy Investment Co., Ltd., Beijing 100007, China; jinxianlin@guohua.com.cn

* Correspondence: chenyixiao@ncepu.edu.cn; Tel.: +86-132-6115-8371

Academic Editors: Frede Blaabjerg and Yongheng Yang
Received: 11 October 2016; Accepted: 2 December 2016; Published: 9 December 2016

Abstract: Since renewable energy resource is universally accepted as a promising method to solve the global energy problem, optimal planning and utilization of various distributed generators (DG) and energy storage (ES) devices deserve special concern. ES devices possess various characteristics in power density, energy density, response speed (switching speed) and lifetime. Besides, as different load types have various requirements on power supply reliability according to their importance, coordinated planning with consideration of reasonable matching between power source and load can efficiently improve power supply reliability and economic efficiency via a customized power supply and compensation strategy. This paper focuses on optimization of power source capacity in microgrid and a coordinated planning strategy is proposed with integrated consideration of characteristics of DG, ES and load. An index named additional compensation ratio (*ACR*) for balancing economic efficiency and reliability is proposed and considered in the strategy. The objective function which aims to minimize life cycle cost (LCC) is established considering economic efficiency, reliability and environmental conservation. The proposed planning strategy and optimizing model is calculated and verified through case study of an autonomy microgrid.

Keywords: microgrid; distributed generation; super capacitor; battery energy storage system (BESS)

1. Introduction

With the increasing demand on energy resources, human society is confronted with significant issues including fossil resource exhaustion, climate change and pollutant emission. In recent decades, renewable energy resources (RER) such as wind and solar energy attracted world-wide attention for their merits in energy conservation as well as in reducing pollutant emission. It is highly recognized that utilization of RER will be one of the most promising methods to solve the global energy problem and achieve sustainable development [1,2].

The distributed integration of wind and solar power helps to reduce loss from long-distance transmission and is a significant method of RER utilization, but the intermittency and fluctuation of wind and solar energy will inevitably influence power supply reliability. Besides, the imbalance between the amount of generation and the load demand may result in power system instability [3]. Hence energy storage (ES) devices, including lead-acid batteries, Li-ion batteries, super capacitor (SC), flywheel storage and superconducting magnetic energy storage (SMES) can be utilized for output power smoothing. A small power system consisting of power converter-based generation, ES devices, small classic synchronous generation, and various types of loads forms a microgrid (MG) [4]. While a number of research works on MG have been done on various aspects, including

control strategy [5–10], energy management systems [11–17], marketing policies [18–21] and system design [22–27], this paper mainly focuses on the optimal sizing of Distributed Energy Resources (DERs), especially the capacity of ES devices in MG.

Power source optimization of MG is basically done by minimizing economic cost while the reliability is guaranteed [28,29]. A number of existing works are done with consideration of complementarity among various power sources as well as source-load coordination. In [25], both reserve sizing problem and loss of load probability (LOLP) index are integrated into the existing storage sizing problem and a probabilistic model is established to strive for a trade-off between reserve cost, storage cost and selling profit. The relationship between storage capacity, reserve capacity and LOLP index is obtained for decision-making on balancing financial cost and reliability. The planning framework proposed in [26] takes into consideration the various characteristics of ES as well as the availability of different renewable energies. The case illustrated in that work adopts hour-level data and emphasized the influence on optimization result caused by variation of diesel generation capacities. The authors of [27] propose a method for coordinated sizing of energy storage (ES) and diesel generators in an isolated microgrid based on discrete Fourier transform. The power fluctuation is decomposed into high-frequency component and low-frequency component, then ES and diesel generators are assigned to these two parts of power correspondingly for power smoothing according to their respond characteristics. The authors of [30] proposed an optimal sizing method of a Vanadium Redox battery in MG and the cost-effective solution is obtained based on the optimal ratings for the battery in both short-term (one-day) and long-term (entire year) scenarios proposed in the paper.

ES devices in the above papers basically involve battery energy storage, while other types of ESs, as well as hybrid energy storage systems (HESS), are discussed in some other works. In [31], the authors proposed a super capacitor energy controller (SCEC) and presented a method for selection of the SCEC and filter parameters as well as precise sizing of the super capacitor for a given application. Battery lifetime is extended by diverging the high-frequency power variations to the super capacitor, and the size of the super capacitor is significantly lower than the one estimated for the traditional super capacitor voltage controller. The authors of [32] investigated the mathematical model and the topology of a HESS based on superconducting magnetic energy storage (SMES) and battery, and a novel system-level control strategy for reasonable and effective power allocation between SMES and battery is proposed. In [33], the authors presented a methodology to size flywheel energy storage for grid-level applications using an optimal control law, which performs trade-offs between minimizing grid power consumption and flywheel energy storage size. The characteristics of flywheel—such as high efficiency, high power density and high self-discharge rate—are considered in the methodology, and case study in this work indicates that the flywheel reduced peak grid power by 8%.

In these works, load is normally considered as a whole and power fluctuation is decomposed into high-frequency component and low-frequency component for power dispatch among ES devices in a HESS. However, different consumers are not equally important and have various requirements on power supply reliability. The authors of [34,35] proposed the classification of load based on importance and the corresponding requirements on power recovery time. For instance, power outage longer than 200 ms is not acceptable for extremely important load (level 1 load); hence, fast-respond energy compensation devices shall be utilized to ensure uninterrupted power supply. In this aspect, although characteristics including power/energy density, efficiency and self-discharge rate are already discussed in existing works on power source sizing of microgrid, the respond speed or switching time of various compensation devices, including ES and diesel generator, are seldom considered.

In order to obtain a reasonable planning scheme with integrated consideration of both power source and load characteristics, analysis and discussion on ES respond speed and load classification is done in this paper. The paper then focuses on the source–load matching mechanism with analysis on economic loss caused by power outage, and a capacity planning strategy considering combinations of ES devices is proposed and an *ACR* index is used for balancing economic efficiency and reliability. With differentiated allocation of capacity of ES devices according to load importance, economic

efficiency can be improved by slightly sacrificing the supply reliability of level 2 and level 3 load, which are less important.

The rest of this paper is organized as follows. In Section 2, modeling of distributed energy resources as well as major characteristics of ES devices are introduced. In Section 3, the source–load matching mechanism and capacity planning strategy are proposed. The objective function based on life cycle cost (LCC) theory is established in Section 4 and case study on an autonomy microgrid is introduced in Section 5.

2. Modeling of Distributed Energy Resources (DERs)

2.1. Modeling of Distributed Generators

The model of a wind turbine (WT) is derived from its power output curve, as illustrated in Figure 1. Though the curve of each type of wind turbine is slightly different from others', they can be generally represented as a piecewise function [36].

$$P_{\mathrm{WT}} = \begin{cases} 0 & 0 \le v < v_{\mathrm{i}} \text{ or } v > v_{\mathrm{o}} \\ a_1 v^3 + a_2 v^2 + a_3 v + a_4 & v_{\mathrm{i}} \le v < v_{\mathrm{r}} \\ P_{\mathrm{r}} & v_{\mathrm{r}} \le v \le v_{\mathrm{o}} \end{cases} \tag{1}$$

where P_{WT} is the output power of wind turbine (WT), P_{r} is the rated power of WT, v_{r} is the rated wind speed of WT, v_{i} is the cut-in wind speed of WT, v_{o} is the cut-out wind speed of WT, a_1~a_4 are coefficients.

The output power of a photovoltaic (PV) panel array is determined by variables including P_{r}, R_{c}, R_{r}, T_{c}, T_{r} and k [37].

$$P_{\mathrm{PV}} = n_{\mathrm{PV}} P_{\mathrm{r}} \left(\frac{R_{\mathrm{c}}}{R_{\mathrm{r}}}\right)[1 + k(T_{\mathrm{c}} - T_{\mathrm{r}})] \tag{2}$$

where P_{PV} is the output power of PV panel array, P_{r} is the rated power of a single PV unit under standard conditions, R_{c} is the current sunlight intensity, R_{r} is the rated sunlight intensity under standard conditions, T_{c} is the current temperature, T_{r} is the rated temperature under standard conditions, k is the power temperature coefficient, n_{PV} is the number of units in the PV panel array.

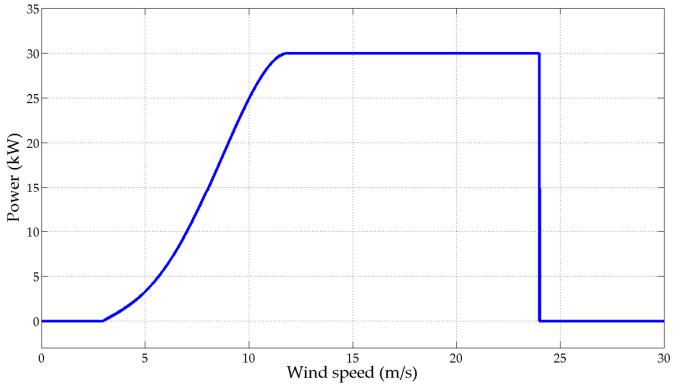

Figure 1. Power output curve of wind turbine (WT).

2.2. Modeling and Characteristic Analysis of Energy Storage Devices and Back-Up Source

ES devices and back-up source are used to compensate energy shortage caused by insufficient distributed generator (DG) generation, hence relative analysis is significant for further study on source–load coordination mechanism. Table 1 shows the characteristics of both energy-type and power-type ES devices, including energy density, power density, investment cost, approximate cycle times and response speed.

Table 1. Parameters of various types of energy storage (ES) devices.

ES Type		Energy Density (Wh/kg)	Power Density (W/kg)	Investment Cost ($/kWh)	Cycle Times	Response Speed
Energy type	Lead-acid battery	30~50	75~300	70~420	10^3	medium
	Li-ion battery	75~250	150~315	280~1400	10^3	medium
Power type	Super capacitor	0.1~15	500~5000	420~5600	10^5	fast
	Flywheel	5~130	400~1600	1400~4900	10^6	fast
	SMES	0.5~5	500~2000	980~9800	10^6	fast

Through observation, it is obvious that two types of ES devices are complementary to each other, and a hybrid storage system can provide enhanced power supply capability. Besides, although flywheel storage and SMES have outstanding performance, they are relatively expensive and are still in the experimental stages, which made them unsuitable for practical application. In this paper, the HESS consists of a lead-acid battery, Li-ion battery and super capacitor.

1. Energy state model of ES device

The operation status of all ES devices can be generally described via the following formula [38,39]:

$$E_{\mathrm{ES}}^{(t)} = E_{\mathrm{ES}}^{(t-1)}(1-\sigma) + P_{\mathrm{ES}}^{(t)} \cdot \eta \cdot \Delta t \tag{3}$$

where $E_{\mathrm{ES}}{}^{(t)}$ is the remaining energy of the ES device at moment t, σ is the self-discharge rate, $P_{\mathrm{ES}}{}^{(t)}$ is the charge/discharge power during time interval t, η is the charge/discharge efficiency, Δt is the duration of time interval.

The energy state of the ES device is determined by E_{ES} at the start of a time interval and charged/discharged power during that period. For different ES devices, the self-discharge rate can vary from 0.1%–0.3%/d (batteries) to 20%–40%/d (super capacitor).

2. Lead-acid battery lifetime model

The lifetime of a lead-acid battery is relatively short and is significantly influenced by operation conditions compared to super capacitors and a Li-ion battery. While the lifetime of super capacitor (SC) can extend as long as 20 years and a Li-ion battery can be charged/discharged for over 5000 cycles, substitution of a lead-acid battery may be required, which makes the lifetime calculation model of batteries essential for optimization of MG source planning.

An existing lifetime calculation model [37] is applied to predict the lifetime of lead-acid batteries. The cycle time of lead-acid batteries is related to depth of discharge (DOD), as illustrated in Figure 2.

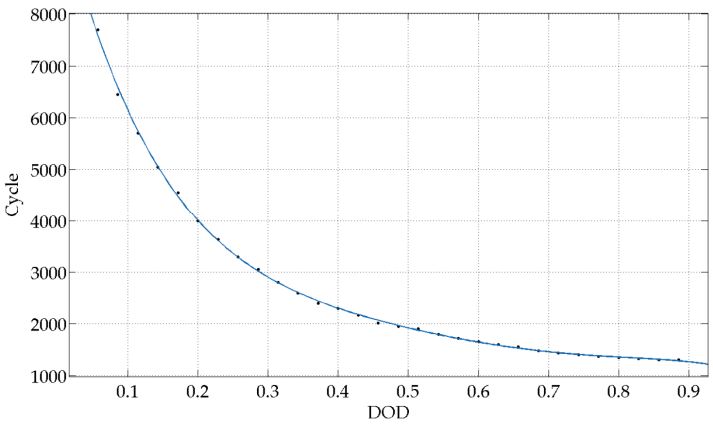

Figure 2. Cycle time of lead-acid batteries. DOD, depth of discharge.

The calculation formula can be expressed as:

$$N = a_1 + a_2 e^{a_3 D_N} + a_4 e^{a_5 D_N} \tag{4}$$

where D_N is the depth of discharge, N is the equivalent cycle times under D_N, a_1~a_5 are coefficients.

The cost of a single charge/discharge cycle is represented as:

$$C_{\text{cycle}} = \frac{C_{\text{cap-B}}}{N} \tag{5}$$

where $C_{\text{cap-B}}$ is the Capital investment of batteries, C_{cycle} is the cost of a single charge/discharge cycle.

Related studies [40,41] indicate that the cumulative lifetime of a battery is influenced by the state of charge (SOC) under which the battery is operating. Besides, a battery may not experience a fixed and whole charge-discharge cycle. Hence, the operation cost model for both the charging and discharging processes, considering the influence caused by SOC, is given in [37].

- Charging process

An influence factor λ_c is introduced to represent the influence on operation cost caused by SOC:

$$\lambda_c = \frac{k_c S_{\max}}{S_{\text{c-start}} S_{\text{c-end}}} \tag{6}$$

where $S_{\text{c-start}}$ is the SOC at the start of the charging process, $S_{\text{c-end}}$ is the SOC at the end of the charging process, k_c is the adjustment coefficient to fix the final value of λ_c.

The cost of a single charging process is then shown by the following equation:

$$C_{c1} = \lambda_c \frac{C_{\text{cap-B}}}{2N} \tag{7}$$

where C_{cl} is the cost of a single charging process, λ_c is the influence factor representing SOC's influence on C_{cl}.

- Discharging process

An influence factor λ_d is introduced to represent the influence on operation cost caused by SOC:

$$\lambda_d = \frac{k_d S_{\text{d-start}}}{S_{\text{d-end}} S_{\max}} \tag{8}$$

where $S_{\text{d-start}}$ is the SOC at the start of the discharging process, $S_{\text{d-end}}$ is the SOC at the end of the discharging process, k_d is the adjustment coefficient to fix the final value of λ_d.

The cost of a single discharging process is then represented as:

$$C_{d1} = \lambda_d \frac{C_{\text{cap-B}}}{2N} \tag{9}$$

where C_{dl} is the cost of a single charging process, λ_d is the influence factor representing SOC's influence on C_{dl}.

3. Fuel consumption model of a diesel generator

The fuel consumption model of a diesel generator is obtained through fitting the fuel consumption curve [42]:

$$C_{\text{Diesel}} = A \times P_G + B \times P_r \tag{10}$$

where C_{Diesel} is the amount of consumed fuel, P_G is the generated power of diesel generator, P_r is the rated power of diesel generator, A and B are coefficients.

3. Analysis of Power Source and Load Coordination Mechanism

3.1. Load Character Analysis

Load in a microgrid consists of different types including: industrial load; commercial load; hospitals; schools; residential load, etc. Different types of load possess unique characteristics and various requirements on power supply reliability. Basically, load can be divided into three categories according to the importance grade. The classification rule of each load grade is regulated in [34], as illustrated in Table 2.

Table 2. Classification of load based on their importance.

Load Grade	Level 1	Level 2	Level 3
Description	Power supply interrupt may cause: casualty; extremely severe pollution; poisoning, explosion or fire; extremely severe political effect; extremely severe economic loss; massive social chaos.	Power supply interrupt may cause: serious pollution; serious political effect; serious economic loss; areal social chaos.	Load not belonging to first class and level 2 load
Supply requirement	Must be supplied without interruption	Should be supplied with minimal interruption	Can be interrupted if necessary

The analysis on the power supply reliability requirement of each load grade is essential for the study on the power-source coordination mechanism. Herein, the time limit of power interruption ($t_{\text{interrupt}}$) is used to measure the reliability requirement of load. This index describes the maximum acceptable power interruption time during a power outage failure. The $t_{\text{interrupt}}$ varies among specific types of each load grade. For instance, $t_{\text{interrupt}}$ of electrical equipment utilized in the electronics manufacturing industry is illustrated in Table 3.

Table 3. $t_{\text{interrupt}}$ of electrical equipment in the electronics manufacturing industry.

Specific Type of Level 1 Load	Electrical Equipment	$t_{\text{interrupt}}$
Electronics manufacturing (Chip manufacturing)	Emergency illumination	≤1 min
	Fire protection facilities	≤1 min
	Information Technology Computer Integrated Manufacturing (IT CIM) equipment	≤200 ms
	Automatic board feeder	≤200 ms
	Tin scraping machine	≤200 ms
	Solder paste printer	≤200 ms
	High-speed chip mounter	≤200 ms
	High-speed welding furnace	≤200 ms

For simplification, $t_{\text{interrupt}}$ of a certain type of load is selected as the minimum value among the $t_{\text{interrupt}}$ of each type of electrical equipment. For instance, $t_{\text{interrupt}}$ of the electronics manufacturing industry is selected as 200 ms. $t_{\text{interrupt}}$ of major types of level 1 load is illustrated in Table 4.

As illustrated above, $t_{\text{interrupt}}$ of major types of level 1 load ranges from several hundred milliseconds up to 1 min. According to the characteristics of ES devices analyzed in Section 2.2, fast responding ES devices, i.e., super capacitor, shall be considered for improving the power supply reliability.

As regards level 2 and level 3 load, the time limit of power interruption is not specified in existing manuals, regulations and national standards. Hence, the power supply reliability of these loads is restricted by the annual power outage limit, as well as by considering energy shortage compensation during life cycle cost (LCC) calculation.

Table 4. $t_{\text{interrupt}}$ of major types of level 1 load.

Types of Level 1 Load		$t_{\text{interrupt}}$
Industrial load	Mining	≤200 ms
	Chemical industry	≤200 ms
	Metallurgic industry	≤1 s
	Electronics manufacturing	≤200 ms
Social load	Communication	≤800 ms
	Radio and television	≤800 ms
	Information safety	≤800 ms
	Public services	≤1 min
	Transportation	≤800 ms
	Medical services	≤0.5 s
	Assembly occupancies	≤1 min

A sector customer damage function (SCDF) to calculate power outage loss is proposed in [43], and the economic loss of a typical load is illustrated in Figure 3. For level 1 load, i.e. industrial load, the economic loss will rise significantly within several minutes after the outage. Hence, the interrupt time shall be limited within the minute level to avoid massive economic loss. For level 2 and level 3 load, the curve increases approximately linearly; this part of the loss is calculated and added to the life cycle cost of the project.

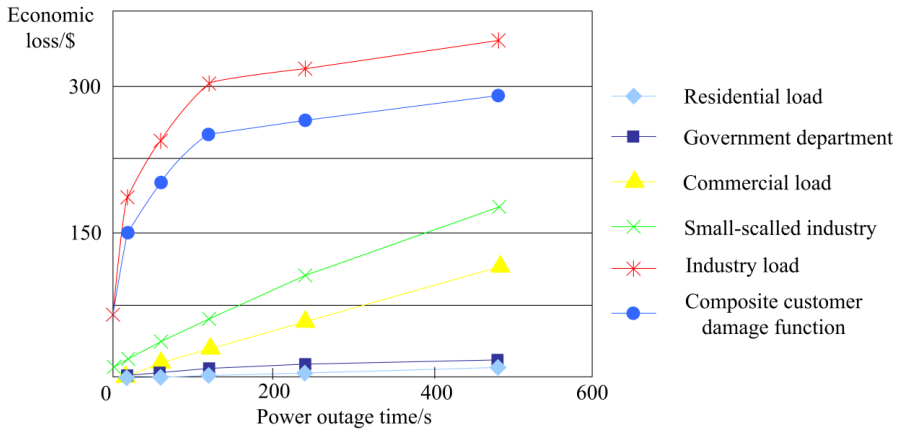

Figure 3. Economic loss curve of typical load after power outage.

3.2. Power Source Capacity Planning Strategy Considering Source-Load Coordination

According to the discussion in Section 3.1, the energy shortage of level 1 load shall be fully compensated at all costs. In order to achieve uninterrupted power supply even if power generation is not sufficient, ES devices and backup sources shall be coordinated according to their response speed, discharge durations and other characteristics. Hence, super capacitors with fast response speed are utilized for smoothing short-time fluctuation or power supply during the initial stage of a long-term energy shortage, while a battery energy storage system (BESS) will successively be utilized for subsequent supply. In extreme cases with intensively long shortage duration, backup sources such as a diesel generator will operate as a stable power source until renewable energy generation is restored.

As for level 2 load, the requirement on power supply reliability is not as strict compared to level 1 load; thus, a short-time outage at the initial stage of a shortage period is acceptable in most cases and investment on SC can then be reduced. When it comes to level 3 load, BESS capacity can also be reduced since level 3 load basically has no requirement on power supply reliability. The principle of source-load coordination is illustrated in Figure 4.

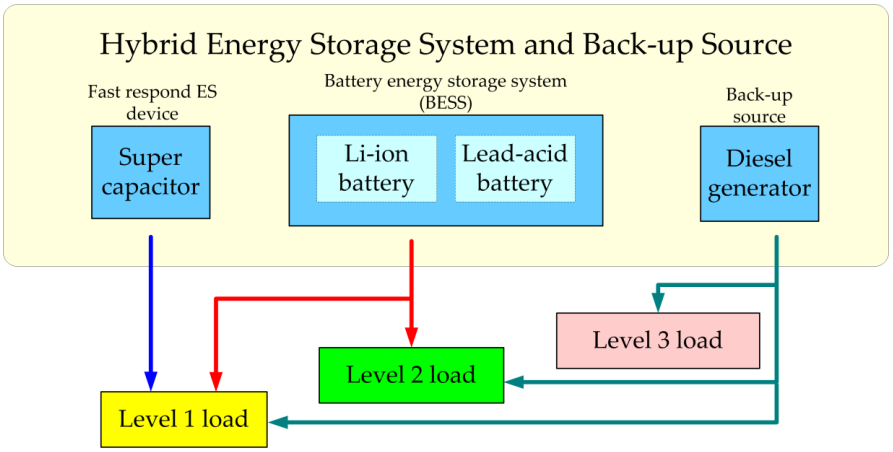

Figure 4. Principle of source-load coordination. ES, energy storage.

BESS in this research consists of a Li-ion battery and a lead-acid battery. Compared to a lead-acid battery, a Li-ion battery has advantages including: (a) relatively high energy density; (b) longer lifetime at high depth of discharge (DOD); (c) high power receiving capability to realize high current charging in a short time, while the charging current of a lead-acid battery is usually limited within 0.25 C to avoid capacity degradation. Nevertheless, the unit cost of a Li-ion battery can be 5~7 times higher than a lead-acid battery, which is the major factor restricting its application. A reasonable portion of a Li-ion battery in BESS, which is charged and discharged with priority, will significantly reduce the utilization frequency of a lead-acid battery and extend the overall lifetime of BESS.

Through surveying typical daily load and climate parameters including temperature, sunlight intensity and wind speed, the curves of load and generated power of wind turbine (WT) and photovoltaic (PV) can be obtained. The difference of generated power and load is then defined as ΔP, and the area enclosed by the ΔP curve and the axis is ΔE_i. Whether ΔE_i is a positive or negative value determines the operation status of ES devices (charging or discharging) during this time interval. $t_{\text{B-switch}}$ and $t_{\text{D-switch}}$ represents the response speed, or switching time, for BESS and diesel generator respectively.

The overall compensation strategy is arranged as follows:

1. Charging process

For a certain time interval with a duration of t_i, if $\Delta E_i > 0$, ES devices will be charged. The redundant energy generated by WT and PV shall firstly be used to charge the SC in order to guarantee energy reserve of fast response ES for uninterrupted supply of level 1 load. BESS will then be charged if energy still remains, i.e., ΔE_i-($E_{\text{SC-max}}$-$E_{\text{SC-available-}i}$) > 0 (Figure 5a).

2. Discharging process

For a certain time interval t_i, if $\Delta E_i < 0$, ES devices will discharge to supplement the energy shortage of load. The time intervals are classified into three categories:

For $t_i < t_{\text{B-switch}}$, SC is utilized for supplementary and the available capacity of SC is used for supplying all level 1 load and a part of level 2 and level 3 load.

For $t_{\text{B-switch}} < t_i < t_{\text{D-switch}}$, SC and BESS will both be utilized. SC will be switched in immediately and discharge until $t_{\text{B-switch}}$, when BESS is ready to switch in, then BESS is used for supplying all level 1 and level 2 load as well as a part of level 3 load.

For $t_i > t_{\text{D-switch}}$, SC will be switched in immediately and discharge until $t_{\text{B-switch}}$, when BESS is ready to switch in. Then the batteries will discharge until $t_{\text{D-switch}}$, when diesel generators are ready to be switched in, then a diesel generator is used for supplying all level 1, level 2 and level 3 load (Figure 5b).

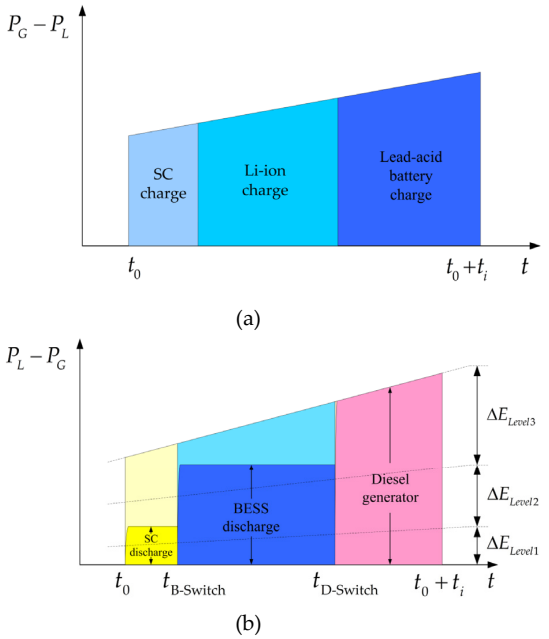

Figure 5. Operation status and coordination strategy of power sources in different conditions. (**a**) Illustration of charging process; (**b**) Illustration of discharging process. SC, super capacitor.

A flowchart of the proposed strategy is illustrated in Figure 6.

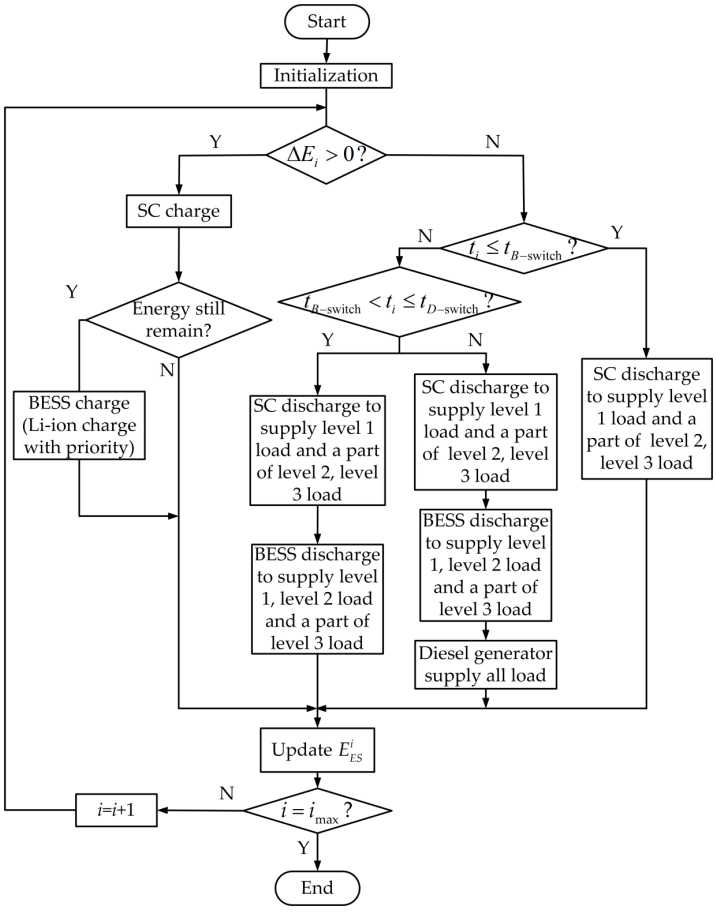

Figure 6. Flowchart of the planning strategy.

Further explanation on discharge strategy is illustrated in Figure 7. For each time interval, the energy shortage is divided into three stages distributed along the time axis in Figure 7a. Each stage of energy shortage consists of forced-compensated part, optional compensated part and abandoned part, as illustrated in Figure 7b.

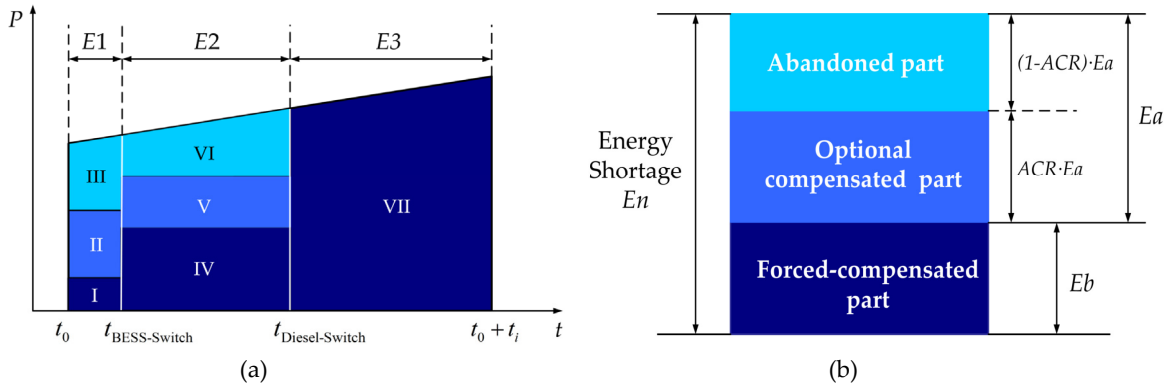

Figure 7. Illustration of discharge strategy with additional compensation ratio (*ACR*) considered. (**a**) Stages of energy shortage; (**b**) Three parts of an energy shortage stage. *ACR*, additional compensation ratio.

Forced-compensated part is the part of energy shortage which must be supplied by energy storage (ES) considering the supply requirement in Table 2. On this basis, additionally compensated energy shortage, which is an optional compensated part for ES, helps to increase the supply reliability. The uncompensated part of energy shortage is considered the abandoned part. Herein, an index named "additional compensation ratio" (*ACR*) is proposed for balancing economic efficiency and reliability. It represents the ratio of optional compensated part for each stage of energy shortage. Optimal *ACR* is obtained through calculation of energy shortage compensation cost C_1.

$$C_{1\text{-}i} = (1 - ACR) \cdot E_a \cdot c_1 + E_{1\text{-}b} \cdot c_2 \tag{11}$$

$$E_a = E_n - E_b, n = 1, 2, 3 \tag{12}$$

where E_n represents each stage of energy shortage in a time interval; E_b is the forced-compensated part of E_n and shall be compensated at all costs. Uncompensated energy $E_{1\text{-}b}$ in this part will be punished with c_2, which has an extremely high value. The abandoned part of energy shortage is considered and calculated with c_1, which is relatively small. The components of each part of energy shortage stages are illustrated in Table 5.

Table 5. Component of each stage of energy shortage.

Stage		Component	Stage		Component	Stage		Component
E_1	I	Level 1 load	E_2	IV	Level 1 and level 2 load	E_3	VII	Level 1, level 2 and level 3 load
	II	Part of Level 2 and Level 3 load		V	Part of Level 3 load			
	III	The rest of Level 2 and Level 3 load		VI	The rest of Level 3 load			

4. Optimized Planning of MG Power Source Capacity

4.1. Objective Function

In order to obtain a scientific and economic efficient scheme of a microgrid planning, an integrated consideration of both long-term costs—including operation as well as maintenance cost—and short-term construction investment is included in this research. The objective function of MG source capacity optimization is set to minimize the economic cost considering life cycle cost (LCC) of the

project. In this model, the LCC optimization theory is applied to take into consideration each part of the cost incurred during the entire duration of the MG project, including the capital investment C_{cap}, the operation and maintenance cost C_{om}, the recycling profit of scrapped equipment C_{r}, the pollutant emission compensation cost C_{p} and the energy shortage compensation cost C_{l}, i.e.,

$$\min C = C_{\text{cap}} + C_{\text{om}} + C_{\text{r}} + C_{\text{p}} + C_{\text{l}} \tag{13}$$

$$C_{\text{cap}} = \sum_{i=1}^{m} \sum_{k=0}^{k_i} N_i \cdot c_i \cdot \frac{1}{(1+r)^{k \cdot L_i}} \tag{14}$$

$$C_{\text{om}} = \sum_{i=1}^{m} \sum_{j=1}^{j_{\max}} C_{\text{om-}i} \cdot \frac{1}{(1+r)^{j}} \tag{15}$$

$$C_{\text{r}} = \sum_{i=1}^{m} \sum_{k=1}^{k_i} c_{\text{r-}i} \cdot \frac{1}{(1+r)^{k \cdot L_i}} \tag{16}$$

$$C_{\text{p}} = \sum_{i=1}^{m} \sum_{j=1}^{j_{\max}} N_{\text{p-}i} \cdot c_{\text{p-}i} \cdot \frac{1}{(1+r)^{j}} \tag{17}$$

$$C_{\text{l}} = \sum_{i=1}^{m} \sum_{j=1}^{j_{\max}} c_{\text{l-}i} \cdot \frac{1}{(1+r)^{j}} \tag{18}$$

where N_i is the amount of i-th DG/ES unit, c_i is the unit price of i-th equipment, k_i represents the replacement times of i-th equipment, L_i is the service time of i-th equipment, r is the discount rate, $c_{\text{om-}i}$ is the annual operation and maintenance cost of i-th equipment, $j_{\max}$ is the service lifetime of the project, $c_{\text{r-}i}$ is the recycling profit of equipment i, $N_{\text{p-}i}$ is the annual emission amount of i-th pollutant, $c_{\text{p-}i}$ is the unit cost of i-th pollutant compensation, $c_{\text{l-}i}$ is the annual energy shortage compensation cost of level i-th load.

4.2. Constrains

1. Constrains of output power of PV, WT and diesel generator:

$$0 \le P_{\text{PV}} \le P_{\text{PV-peak}} \tag{19}$$

$$0 \le P_{\text{WT}} \le P_{\text{r}} \tag{20}$$

$$P_{\text{diesel-min}} \le P_{\text{diesel}} \le P_{\text{diesel-max}} \tag{21}$$

   For PV and WT, the limits (especially for minimum values) are associated with the primary source.

2. Constrains of charge and discharge power of ES devices:

$$\begin{cases} P_{\text{c-min}} \le P_{\text{ES}} \le P_{\text{c-max}} \\ P_{\text{d-min}} \le P_{\text{ES}} \le P_{\text{d-max}} \end{cases} \tag{22}$$

   where $P_{\text{c-max}}$, $P_{\text{c-min}}$ are the maximum and minimum charging power of ES devices.

3. Constrains of power supply reliability, where the unserved time of level i-th load ($T_{\text{l-}i}$) shall not exceed its corresponding limit:

$$T_{\text{l-}i} < T_{\text{max-}i} \tag{23}$$

4. Constrains of ES discharging time span, for each discharging process, the discharging time span of SC and battery shall be limited according to the proposed strategy:

$$\begin{cases} t_{\text{SC-discharge}} \leq t_{\text{B-switch}} \\ t_{\text{B-discharge}} \leq t_{\text{D-switch}} - t_{\text{B-switch}} \end{cases} \quad (24)$$

5. Case study

5.1. Parameters

Basic parameters of WT, PV panel, diesel generator, super capacitor and a lead-acid battery are illustrated in Table 6.

Table 6. Basic parameters of power sources.

Distributed Energy Resources (DERs)	Parameter	Value
Wind turbine (WT)	Unit price	\$100,000
	Rated power	30 kW
	Rated wind speed	12 m/s
	Cut-in wind speed	3 m/s
	Cut-out wind speed	24 m/s
Photovoltaic (PV) unit	Unit price	\$90
	Rated power	0.2 kWp
	Rated sunlight intensity	1 kW/m^2
	Ratedtemperature	25 °C
	Power temperature coefficient	−0.45%
Diesel generator	Unit price	\$5000
	Rated power	100 kW
	Coefficient *A*	0.246 L/kWh
	Coefficient *B*	0.08145 L/kWh [1]
Super capacitor (SC)	Unit price	\$7200
	Unit capacity	1 kWh
Li-ion battery	Unit price	\$2.1
	Unit capacity	3.2 V 3000 mAH
Lead-acid battery	Unit price	\$184
	Unit capacity	2 V 1000 Ah
	Coefficients in lifetime model	$a_1 = 0$, $a_2 = 7753$, $a_3 = -7.263$, $a_4 = 2603$, $a_5 = -0.8455$ [2]

[1] The coefficient values are proposed by Skarstein and Ullen [44]; [2] the coefficient values are obtained via curve fitting.

Different ES devices and backup sources possess various switching time characters. As for super capacitor, the switching time can be as short as microseconds (set as 20 ms in this paper). Meanwhile, BESS has a longer switching time compared to super capacitor, set as 1 min in this paper, via integrated consideration of component character and power quality requirement. For diesel generators, a warm-up process is required before supplying regulated power to the load, normally 40% of the rated power. This time varies according to the ambient temperature, ranging from 4 to 8 min, and can be up to 20~30 min under extreme conditions (i.e., −40 °C temperature). The switching time of the diesel generator is set as 5 min in this paper. It is worth noting that the switching time of all power source devices relies on parameters of the control system and power-electronic converters, hence t_{switch} can be adjusted and modified accordingly in specific applications and this research aims to propose a generic approach.

5.2. Load Character and DER Data

To verify the proposed optimization strategy and method, a microgrid project with a 20-year service lifetime is selected as an example. Load in this microgrid project consists of level 1 load

(industrial load, government department, hospital, telecommunication facility), level 2 load (schools, commercial load), level 3 load (residential load). With a general consideration of power balance in the system, renewable energy resource applied in the grid consists of 14 × 30 kW wind turbines and 48 kWh photovoltaic panels. The typical daily load curves are illustrated in Figure 8. The renewable energy generation curve is illustrated in Figure 9 according to the environment data illustrated in Table 7.

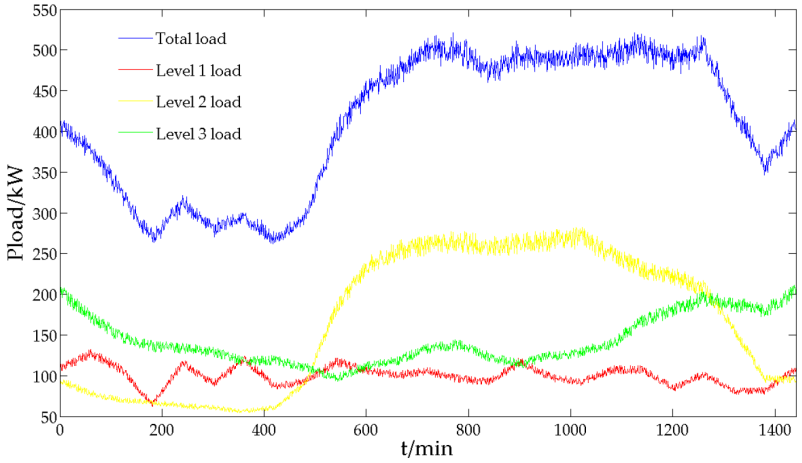

Figure 8. Typical daily load curves.

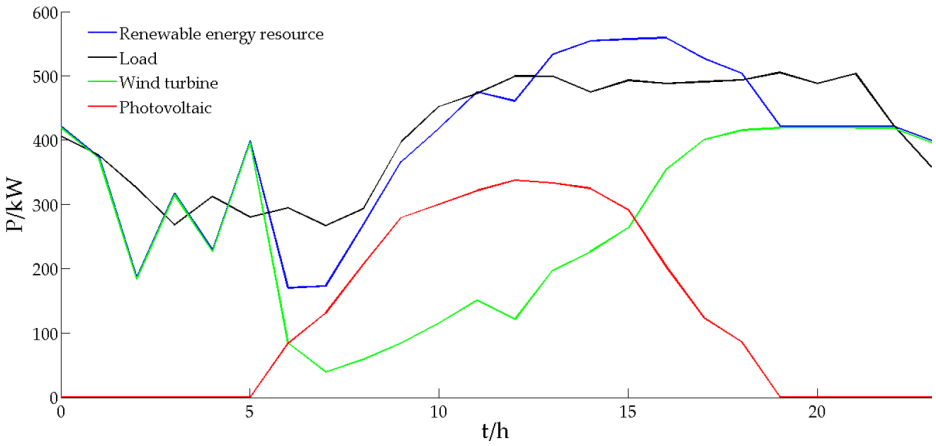

Figure 9. Renewable energy generation curves.

Table 7. Environmental data.

Time	Wind Speed (m/s)	Sunlight Intensity (KW/m^2)	Temperature (°C)	Time	Wind Speed (m/s)	Sunlight Intensity (KW/m^2)	Temperature (°C)
0	12	0	16	12	6.7	0.83	18.4
1	10.4	0	15.2	13	7.9	0.82	18.6
2	7.7	0	14.5	14	8.3	0.8	18.6
3	9.5	0	14.4	15	8.8	0.72	19.5
4	8.3	0	13.8	16	10.1	0.5	19.2
5	10.9	0	13.3	17	11	0.303	18.6
6	6	0.2	13.1	18	11.5	0.21	18
7	4.8	0.315	13.5	19	12	0	17.3
8	5.4	0.5	14.2	20	12	0	17.1
9	6	0.68	15.7	21	12	0	16.9
10	6.6	0.735	17.1	22	11.8	0	16.3
11	7.2	0.79	18.2	23	10.9	0	15.8

Based on the illustrated data, C_{om} of a typical day can be obtained, and annual costs for operation and maintenance are calculated as $365C_{om}$. Annual pollutant compensation and energy shortage compensation cost is obtained similarly. The recycling profit C_r is calculated as 5% of the capital investment cost for each type of device, and the scrap value at the ending year of lifetime is discounted into the value at the initial year with r = 3%.

5.3. ES Device Capacity Optimization

Particle Swarm Optimization (PSO) algorithm is applied to solve this problem. PSO algorithm is an evolutionary algorithm proposed by Kennedy J. and Eberhart R. in 1995 [45], and attracted extensive attention for its advantages in easy application, high precision and convergence speed. In this case, algorithm parameters are set as: iterations I_{max} = 1000; maximum speed V_{max} = 50; population size m = 20. I_{max} is set to avoid the iterative process being trapped into a loop, and the iterations will stop when no improvement (larger than 10^{-5}) has occurred in the last 100 iterations [46].

The optimized LCC result of this planning scheme is \$1,594,127 with ACR = 0.4818; specific results of optimized capacity are shown in Table 8, LCC costs of each device are shown in Table 9 and calculation results of each LCC component are shown in Table 10.

Table 8. Specified optimization result.

Device	Capacity	Lifetime/a	Times of Replacement	Total Cost/\$
Wind turbine	450 kW	20	0	1,400,000
Photovoltaic	48 kW	20	0	21,600
Super capacitor	1.38 kWh	20	0	10,000
Li-ion battery	5.73 kWh	5.87	3	1722
Lead-acid battery	27 kWh	7.13	2	2490
Diesel generator	100 kW	20	0	5000

Table 9. Life cycle costs (LCC) of each device.

Device	Capital Cost/\$	Operation & Maintenance/\$ (Considering Pollutant Emission)	Recycling Profit/\$
WT	1,400,000	109,920	−39,920
PV	21,600	1696	−616
SC	10,000	393	−285
BESS	4212	1662	−346
Diesel	5000	65,219	−143

Table 10. Calculation results of each LCC component.

LCC Component	Cost/\$
C_{cap}	1,440,812
$C_{om} + C_p$	178,879
C_r	−41,310
C_l	15,746

The optimizing curve of LCC is illustrated in Figure 10.

ACR is the ratio of optional compensated part for each stage of energy shortage. It reflects the improvement on supply reliability while basic requirements on power supply for level 1, level 2 and level 3 load are satisfied.

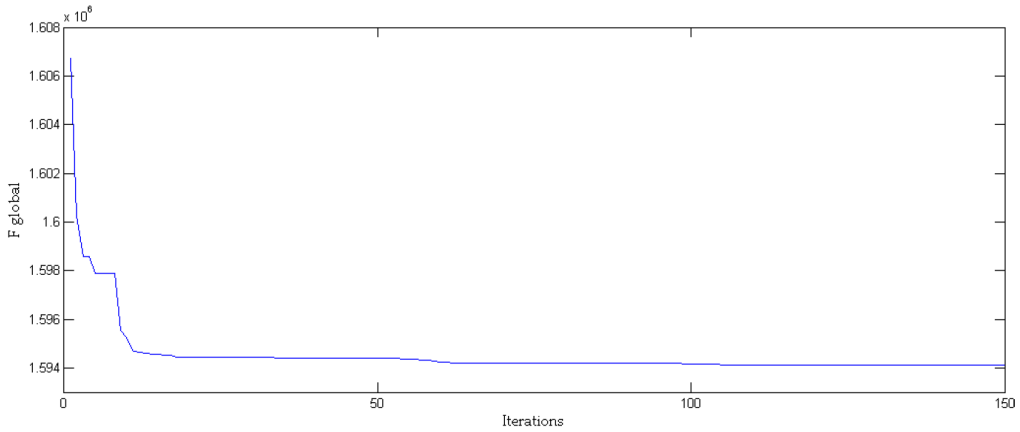

Figure 10. Optimizing curve of life cycle cost (LCC).

When ACR = 0, I, IV, VII in Figure 7 will be compensated while energy shortage of II, III, VI will be abandoned and calculated into compensation cost in C_l, as illustrated in Figure 11.

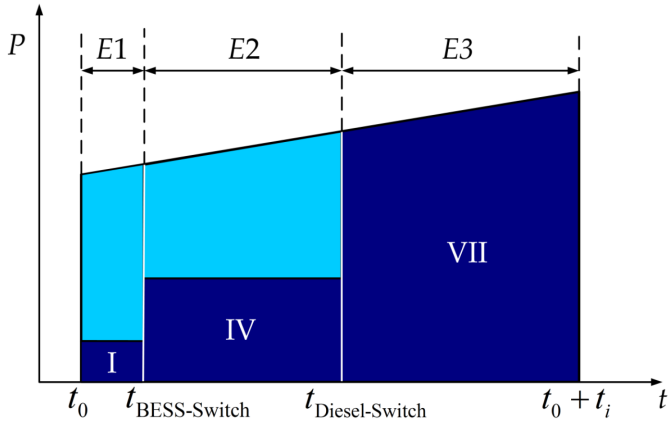

Figure 11. Compensated energy shortage (ACR = 0).

The calculation result is shown in Figure 12.

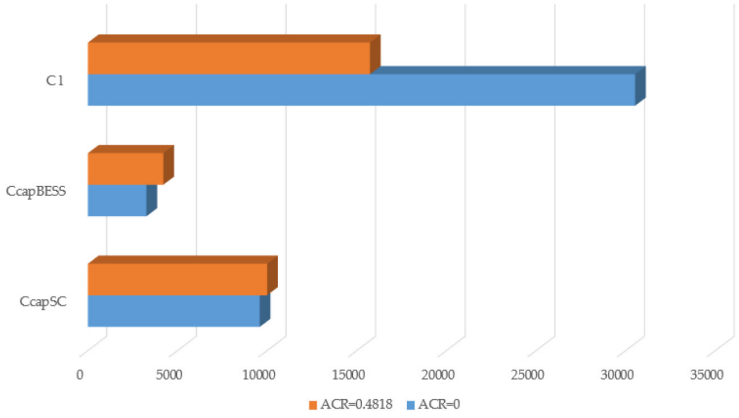

Figure 12. Calculation result at ACR = 0.

As illustrated, although the investment cost of ES devices slightly decreased (C_{capSC} decreased by 4% and $C_{capBESS}$ decreased by 22%) compared with the optimal planning scheme at ACR = 0.4818,

the compensation cost C_1 significantly increased from \$15,746 to \$30,526 by 94%. The LCC result increased from \$1,594,127 to \$1,608,205.

When *ACR* = 1, all parts of energy shortage in Figure 7 (I~VII) will be totally compensated (III, VI are reduced to zero), as illustrated in Figure 13. The compensation cost C_1 is theoretically zero.

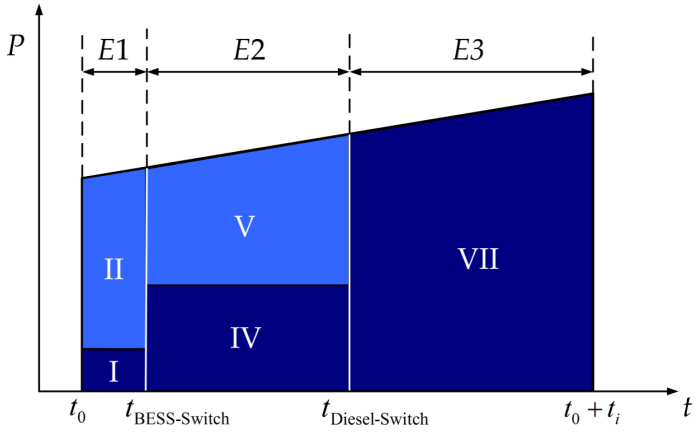

Figure 13. Compensated energy shortage (*ACR* = 1).

The calculation result is shown in Figure 14.

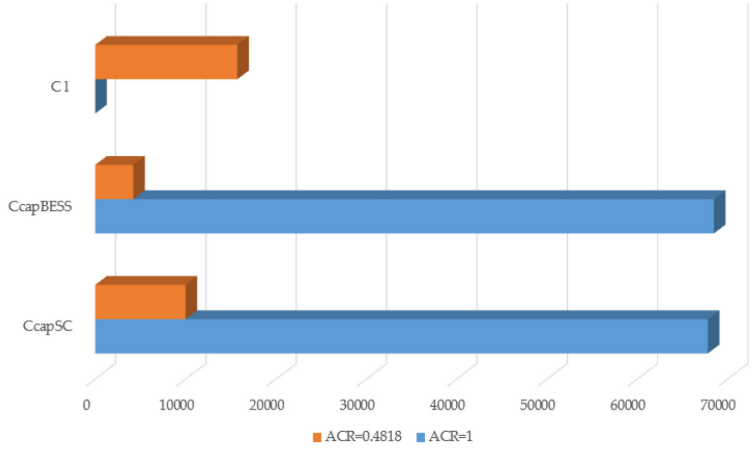

Figure 14. Calculation result at *ACR* = 1.

As illustrated, the compensation cost C_1 is reduced to zero as expected. However, the investment costs of SC and BESS increase approximately 5.8 and 16 times than those of the optimal planning scheme at *ACR* = 0.4818 respectively. The LCC result increases to \$1,774,287.

Based on the above discussion, the proposed *ACR* is the key to balancing economic efficiency and supply reliability. The relationship between *ACR* and optimal cost is illustrated in Figure 15 through calculation and fitting.

Through observation, the optimal planning scheme is obtained at *ACR* = 0.4818, and the cost will increase whether the *ACR* value is too small or too high. The decreasing tendency on the left side occurs because the exceeded compensation cost is reduced by reasonable investment on ES devices, while excessive investment would lead to over-sizing of ESS and the cost rises on the right side of the curve. Moreover, when *ACR* exceeds 0.5, the cost will increase sharply. This phenomenon indicates that improving reliability gradually becomes harder. For instance, improving *ACR* from 0.8 to 0.9 requires a \$42,083 increase in the cost, while only \$23,636 is needed for improving *ACR* from 0.6 to 0.7.

It is easy to achieve good performance, but hard to be perfect. This characteristic can provide guidance for decision-makers to obtain optimal planning schemes under different conditions with particular requirements on reliability and economic efficiency.

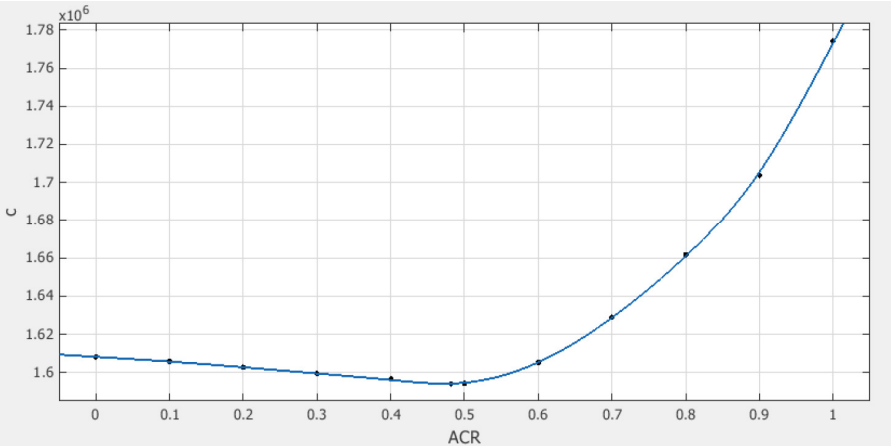

Figure 15. Relationship between *ACR* and optimal cost.

6. Conclusions

In this paper, the character analysis as well as modeling of typical DG and ES devices are completed with special emphasis on ES characters. Load character is considered to obtain a reasonable coordination strategy considering combinations of ES devices and diesel generator, followed by establishing the objective function based on life cycle cost (LCC) calculation. The proposed planning strategy and optimizing model are verified through optimized planning of the energy source capacity of an autonomy microgrid, and is able to ensure power supply for an important load, while maintaining a reasonable economic cost. The relationship between economic cost and the proposed *ACR* index, which reflects supply reliability condition of the system, will help decision-makers to obtain optimal planning schemes under different conditions with particular requirement on supply reliability. Hopefully, this study will provide suggestions for decision making in future power source capacity planning schemes of autonomy microgrid on isolated islands or in remote areas, and the power source coordination strategy can also be used as a reference in DG integration in power systems as well as smart grids. Further work on microgrid structure planning and evaluation methods is already on the agenda; all of these research works will eventually form an integrated, flexible and coordinated system of a microgrid planning method.

Acknowledgments: The authors would like to appreciate the detailed comments of the anonymous reviewers and the kind help of the Editor, which significantly enhanced the quality of the paper. The research work was funded by the National Natural Science Foundation of China (NSFC) (Grant No. 51577058).

Author Contributions: Zifa Liu contributed to the research idea and the framework of this work. Yixiao Chen proposed the planning strategy. Ya Luo established the methectic models. Guankun Zhao and Xianlin Jin performed the case study and analyzed the data. Yixiao Chen wrote the paper.

Conflicts of Interest: The authors declare no conflict of interest.

References

1. Meisen, P. Linking renewable energy resources: A compelling, global strategy for sustainable development. *IEEE Power Eng. Rev.* **1998**, *18*, 16–18. [CrossRef]
2. Xu, Y.; Singh, C. Adequacy and economy analysis of distribution systems integrated with electric energy storage and renewable energy resources. *IEEE Trans. Power Syst.* **2012**, *27*, 2332–2341. [CrossRef]
3. Marzband, M.; Moghaddam, M.M.; Akorede, M.F.; Khomeyrani, G. Adaptive load shedding scheme for frequency stability enhancement in microgrids. *Electr. Power Syst. Res.* **2016**, *140*, 78–86. [CrossRef]

4. Marzband, M.; Azarinejadian, F.; Savaghebi, M.; Guerrero, J.M. An optimal energy management system for islanded microgrids based on multiperiod artificial bee colony combined with markov chain. *IEEE Syst. J.* **2015**, *100*, 1–11. [CrossRef]
5. Solanki, A.; Nasiri, A.; Bhavaraju, V.; Familiant, Y.L.; Fu, Q. A new framework for microgrid management: Virtual droop control. *IEEE Trans. Smart Grid.* **2016**, *7*, 554–566. [CrossRef]
6. Olivares, D.E.; Mehrizi-Sani, A.; Etemadi, A.H.; Canizares, C.A.; Iravani, R.; Kazerani, M.; Hajimiragha, A.H.; Gomis-Bellmunt, O.; Saeedifard, M.; Palma-Behnke, R.; et al. Trends in microgrid control. *IEEE Trans. Smart Grid.* **2014**, *5*, 1905–1919. [CrossRef]
7. Yang, X.; Du, Y.; Su, J.; Chen, X. An optimal secondary voltage control strategy for islanded microgrid. In Proceedings of the IEEE International Power Electronics and Motion Control Conference, Hefei, China, 22–26 May 2016.
8. Li, J.; Li, F.; Li, X.; Liu, H.; Chen, F.; Liu, B. S-shaped droop control method with secondary frequency characteristics for inverters in microgrid. *IET Gener. Transm. Dis.* **2016**, *10*, 3385–3392. [CrossRef]
9. Sun, X.; Hao, Y.; Wu, Q.; Guo, X. A multifunctional and wireless droop control for distributed energy storage units in Islanded AC microgrid applications. *IEEE Trans. Power Electr.* **2016**, *32*, 736–751. [CrossRef]
10. Abdelaziz, M.M.A.; Farag, H.E. An enhanced supervisory control for islanded microgrid systems. *IEEE Trans. Smart Grid.* **2016**, *7*, 1941–1943. [CrossRef]
11. Marzband, M.; Parhizi, N.; Savaghebi, M.; Guerrero, J.M. Distributed smart decision-making for a multimicrogrid system based on a hierarchical interactive architecture. *IEEE Trans. Energy Conver.* **2016**, *31*, 644–655. [CrossRef]
12. Marzband, M.; Sumper, A.; Ruiz-Alvarez, A.; Dominguez-Garcia, J.L.; Tomoiaga, B. Experimental evaluation of a real time energy management system for stand-alone microgrids in day-ahead markets. *Appl. Energy* **2013**, *106*, 365–376. [CrossRef]
13. Marzband, M.; Sumper, A.; Dominguez-Garcia, J.L.; Gumara-Ferret, R. Experimental validation of a real time energy management system for microgrids in islanded mode using a local day-ahead electricity market and MINLP. *Energ. Convers. Manag.* **2013**, *76*, 314–322. [CrossRef]
14. Marzband, M.; Ghadimi, M.; Sumper, A.; Dominguez-Garcia, J.L. Experimental validation of a real-time energy management system using multi-period gravitational search algorithm for microgrids in islanded mode. *Appl. Energy* **2014**, *128*, 164–174. [CrossRef]
15. Marzband, M.; Javadi, M.; Dominguez-Garcia, J.L.; Moghaddam, M.M. Non-cooperative game theory based energy management systems for energy district in the retail market considering DER uncertainties. *IET Gener. Transm. Dis.* **2016**, *10*, 2999–3009. [CrossRef]
16. Marzband, M.; Parhizi, N.; Adabi, J. Optimal energy management for stand-alone microgrids based on multi-period imperialist competition algorithm considering uncertainties: experimental validation. *INT Trans. Electr. Energy.* **2016**, *26*, 1358–1372. [CrossRef]
17. Marzband, M.; Yousefnejad, E.; Sumper, A.; Dominguez-Garcia, J.L. Real time experimental implementation of optimum energy management system in standalone Microgrid by using multi-layer ant colony optimization. *Int. J. Electr. Power Energy Syst.* **2016**, *75*, 265–274. [CrossRef]
18. Zhang, D.; Li, S.; Zeng, P.; Zang, C. Optimal microgrid control and power-flow study with different bidding policies by using powerworld simulator. *IEEE Trans. Sustain. Energ.* **2014**, *5*, 282–292. [CrossRef]
19. Park, S.; Lee, J.; Bae, S.; Hwang, G.; Choi, J.K. Contribution-based energy-trading mechanism in microgrids for future smart grid: A game theoretic approach. *IEEE Trans. IND Electron.* **2016**, *63*, 4255–4265. [CrossRef]
20. Paschalidis, I.C.; Li, B.; Caramanis, M.C. Demand-side management for regulation service provisioning through internal pricing. *IEEE Trans. Power Syst.* **2012**, *27*, 1531–1539. [CrossRef]
21. Misra, S.; Bera, S.; Ojha, T. D2P: Distributed dynamic pricing policy in smart grid for PHEVs management. *IEEE Trans. Parall. Distr.* **2015**, *26*, 702–712. [CrossRef]
22. Arefifar, S.A.; Mohamed, Y.A.R.I.; El-Fouly, T.H.M. Optimum microgrid design for enhancing reliability and supply-security. *IEEE Trans. Smart Grid.* **2013**, *4*, 1567–1575. [CrossRef]
23. Shadmand, M.B.; Balog, R.S. Multi-objective optimization and design of photovoltaic-wind hybrid system for community smart DC microgrid. *IEEE Trans. Smart Grid.* **2014**, *5*, 2635–2643. [CrossRef]
24. Arefifar, S.A.; Mohamed, Y.A.I. DG mix, Reactive sources and energy storage units for optimizing microgrid reliability and supply security. *IEEE Trans. Smart Grid.* **2014**, *5*, 1835–1844. [CrossRef]

25. Dong, J.; Gao, F.; Guan, X.; Zhai, Q.; Wu, J. Storage-reserve sizing with qualified reliability for connected high renewable penetration micro-grid. *IEEE Trans. Sustain. Energ.* **2016**, *7*, 732–743. [CrossRef]
26. Yang, P.; Nehorai, A. Joint optimization of hybrid energy storage and generation capacity with renewable energy. *IEEE Trans. Smart Grid.* **2013**, *5*, 1566–1574. [CrossRef]
27. Xiao, J.; Bai, L.; Li, F.; Liang, H.; Wang, C. Sizing of energy storage and diesel generators in an isolated microgrid using Discrete Fourier Transform (DFT). *IEEE Trans. Sustain. Energ.* **2014**, *5*, 907–916. [CrossRef]
28. Kerdphol, T.; Fuji, K.; Mitani, Y.; Watanabe, M.; Qudaih, Y. Optimization of a battery energy storage system using particle swarm optimization for stand-alone microgrids. *Int. J. Electr. Power Energy Syst.* **2016**, *81*, 32–39. [CrossRef]
29. Mitra, J.; Vallem, M.R.; Singh, C. Optimal deployment of distributed generation using a reliability criterion. *IEEE Trans. IND Appl.* **2016**, *52*, 1. [CrossRef]
30. Nguyen, T.A.; Crow, M.L.; Elmore, A.C. Optimal sizing of a vanadium redox battery system for microgrid systems. *IEEE Trans. Sustain. Energ.* **2015**, *6*, 729–737. [CrossRef]
31. Abeywardana, D.W.; Hredzak, B.; Agelidis, V.; Demetriades, G. Supercapacitor sizing method for energy controlled filter based hybrid energy storage systems. *IEEE Trans. Power Electr.* **2017**, *32*, 1626–1637. [CrossRef]
32. Wang, S.; Tang, Y.; Shi, J.; Gong, K.; Liu, Y.; Ren, L.; Li, J. Design and advanced control strategies of a hybrid energy storage system for the grid integration of wind power generations. *IET Renew. Power Gener.* **2015**, *9*, 89–98. [CrossRef]
33. Hearn, C.S.; Lewis, M.C.; Pratap, S.B.; Hebner, R.E.; Uriarte, F.M.; Chen, D.; Longoria, R.J. Utilization of optimal control law to size grid-level flywheel energy storage. *IEEE Trans. Sustain. Energ.* **2013**, *4*, 611–618. [CrossRef]
34. *Specific Configuration of Power Supply and Self-emergency Power Supply for Important Power Users*; GB/Z 29328-2012; Standards Press of China: Beijing, China, 2013; pp. 15–21.
35. IEEE Recommended Practice for Emergency and Standby Power Systems for Industrial and Commercial Applications. Available online: http://ieeexplore.ieee.org/servlet/opac?punumber=5252 (accessed on 7 December 2016).
36. Bowden, G.J.; Barker, P.R.; Shestopal, V.O.; Twidell, J.W. The weibull distribution function and wind power statistics. *Wind Eng.* **1983**, *7*, 85–98.
37. Jian, C.; Wang, C.; Bo, Z.; Zhang, X. Economic operation optimization of a stand-alone microgrid system considering characteristics of energy storage system. *Autom. Electric Power Syst.* **2012**, *36*, 25–31.
38. Bahramirad, S.; Reder, W.; Khodaei, A. Reliability-constrained optimal sizing of energy storage system in a microgrid. *IEEE Trans. Smart Grid.* **2012**, *3*, 2056–2062. [CrossRef]
39. Atia, R.; Yamada, N. Sizing and analysis of renewable energy and battery systems in residential microgrids. *IEEE Trans. Smart Grid.* **2016**, *7*, 1–10. [CrossRef]
40. Jenkins, D.P.; Fletcher, J.; Kane, D. Lifetime prediction and sizing of lead-acid batteries for microgeneration storage applications. *IET Renew. Power Gen.* **2008**, *2*, 191–200. [CrossRef]
41. Kaiser, R. Optimized battery-management system to improve storage lifetime in renewable energy systems. *J. Power Sources.* **2007**, *168*, 58–65. [CrossRef]
42. Dufo-López, R.; Bernal-Agustín, J.L. Multi-objective design of PV–wind–diesel–hydrogen–battery systems. *Renew. Energ.* **2008**, *33*, 2559–2572. [CrossRef]
43. Wacker, G.; Billinton, R. Customer cost of electric service interruptions. *Proc. IEEE.* **1989**, *77*, 919–930. [CrossRef]
44. Skarstein, O.; Uhlen, K. Design considerations with respect to long-term diesel saving in wind/diesel plants. *Wind Eng.* **1989**, *13*, 72–87.
45. Kennedy, J.; Eberhart, R. Particle swarm optimization. In Proceedings of the IEEE International Conference on Neural Networks, Perth, Australia, 27 November 1995; pp. 1942–1948.
46. Selvakumar, A.I.; Thanushkodi, K. A new particle swarm optimization solution to nonconvex economic dispatch problems. *IEEE Trans. Power Syst.* **2007**, *22*, 42–51. [CrossRef]